Guylaine Hoffner*, William André, Christophe Sandt and Philippe Djian*

# Synchrotron-based infrared spectroscopy brings to light the structure of protein aggregates in neurodegenerative diseases

**Abstract**: The accumulation of misfolded proteins in the form of aggregates characterizes a number of diseases of the central nervous system such as Alzheimer's disease, Parkinson's disease, prion diseases, and the diseases of polyglutamine expansion. Recent evidence obtained *in vitro* and in mice has suggested that protein aggregates are structurally diverse and that their structure largely determines toxicity. The structure of the aggregated proteins in the brain of human patients remains mostly unknown, and we will give here the reasons for which synchrotron-based infrared spectroscopy is emerging as one of the best techniques to access this structure. We will also review the few publications that already exist on the application of synchrotron-based infrared spectroscopy to the study of protein aggregates in human brain. The establishment of a correlation between aggregate structure and neurological toxicity is important not only to understand the aggregation process itself but also in order to specifically target the most toxic structures when searching for prophylactic or therapeutic inhibitors of protein aggregation.

**Keywords:** Alzheimer; amyloid; Huntington; Parkinson; prion.

DOI 10.1515/revac-2014-0016
Received June 3, 2014; accepted October 12, 2014; previously published online November 11, 2014

## Introduction

Neurological diseases associated with the formation of protein aggregates include Alzheimer's disease (AD), Parkinson's disease (PD), prion diseases, some forms of amyotrophic lateral sclerosis (ALS), and the diseases of polyglutamine (polyQ) expansion. AD is the most common neurodegenerative disorder. It is a disease of unknown cause (although there are some familial cases) characterized by cerebral deposition of the amyloid-β peptide (Aβ) in extracellular senile plaques (Kang et al. 1987) and of hyperphosphorylated tau protein in intracellular neurofibrillary tangles (Delacourte and Défossez 1986, Grundke-Iqbal et al. 1986, Kosik et al. 1986). PD associates motor manifestations, including tremor, rigidity, bradykinesia, and postural instability. These symptoms result from the progressive loss of dopamine-producing neurons in the substantia nigra. Affected neurons develop characteristic protein aggregates called Lewy bodies (Lewy 1912). Lewy bodies are also found in neurological diseases other than PD: multiple system atrophy (Spillantini et al. 1998), dementia with Lewy bodies (Lennox et al. 1989), and some forms of AD (Rosenblum and Ghatak 1979). Because the primary component of Lewy bodies is α-synuclein and because the boundary between diseases with Lewy bodies is not always clear (Spillantini et al. 1997), all of these diseases have been grouped in the so-called α-synucleinopathies (Goedert and Spillantini 1998). Prion diseases, also designated transmissible spongiform encephalopathies (TSEs), are generally attributed to an abnormally folded infectious protein (Prusiner 1982), although this has been challenged (Somerville 2002). Human prion diseases include Gerstmann-Straüssler-Scheinker syndrome, Kuru, fatal familial insomnia, Creutzfeldt-Jakob disease (CJD), and variant CJD. The brain of patients with prion diseases is characterized by the accumulation of the prion protein $PrP^{Sc}$, which is a misfolded form of $PrP^{c}$, a 209-amino-acid glycoprotein involved in cell signaling (Hirsch et al. 2014). While $PrP^{c}$ is rich in α-helix, $PrP^{Sc}$ is enriched in β-sheets (Pan et al. 1993). ALS affects the motor neurons of the spinal cord. Although most cases of ALS have no obvious cause, there exists a familial form caused by a dominant mutation in the copper-zinc superoxide dismutase (SOD1) (Rosen et al. 1993). The mutated SOD1 protein forms small aggregates in motor neurons (Bruijn et al. 1997).

***Corresponding authors: Guylaine Hoffner and Philippe Djian,** Brain Physiology Laboratory, Centre National de la Recherche Scientifique, Paris Descartes University, 45 rue des Saints Pères, 75006 Paris, France, e-mail: guylaine.hoffner@parisdescartes.fr; philippe.djian@parisdescartes.fr
**William André and Christophe Sandt:** Synchrotron SOLEIL, 91192 Saint-Aubin, France

The diseases of polyQ expansion differ from the other diseases of protein aggregation in the sense of having a clear and unified cause, which is an unconventional mutation consisting in the expansion of a CAG repeat. As the polyCAG is always located in the coding region, the mutation results in a protein with an abnormally long polyQ sequence (reviewed in Hoffner and Djian 2002). Huntington's disease (HD) is the most frequent of the diseases of polyQ expansion. It results from an excessively long CAG repeat in the first exon of the gene encoding huntingtin (htt), a large protein of unknown function (The Huntington's Disease Collaborative Research Group 1993). In most persons, the polyQ is about 20 residues long. Disease appears when the polyQ exceeds 35–40 residues. A polyQ of 40–65 residues produces the adult form of the disease (AHD), while expansion beyond 60–65 residues usually results in the more severe and less frequent juvenile form (JHD). HD is characterized by the progressive destruction of neurons in the striatum and, to a lesser extent, in the cerebral cortex (Vonsattel et al. 1985). Neurodegeneration is associated with the formation of microscopic aggregates called inclusions, which contain N-terminal fragments of expanded htt (DiFiglia et al. 1997, Hoffner et al. 2005, Landles et al. 2010). Inclusions are mostly nuclear in juvenile patients and cytoplasmic in adult cases (Hoffner et al. 2005). Although protein misfolding and aggregation are recognized as key events in HD, there is still a controversy about the neurotoxicity of the protein aggregates. This controversy springs mainly from the existence in HD brain of inclusions without neuronal death and of neuronal death without inclusions (Saudou et al. 1998, Arrasate et al. 2004, Hoffner and Djian 2014). Recent studies have revealed that protein deposition in HD (and in AD) is a process more complex than previously thought. Each category of aggregates, whether oligomers, fibrils, or inclusions, is structurally heterogeneous (Fändrich 2007, Stefani 2012, Hoffner and Djian 2014). The conformation of htt aggregates depends largely on the context in which they are formed and is influenced by factors such as experimental conditions, subcellular localization, age, length of the polyQ, and whether aggregation develops in an animal or a patient (Nekooki-Machida et al. 2009, Tonoki et al. 2011, André et al. 2013).

Fourier-transform infrared (FTIR) spectroscopy associated with synchrotron radiation has the unique ability to explore the secondary structure of proteins directly in tissues and can thereby be used to study neurological diseases associated with protein misfolding. In the first part of this review, we will present background knowledge on the determination of protein secondary structure by infrared (IR) spectroscopy and on the advantages of using a synchrotron source. We will also summarize the methods used for preparing human tissue to be analyzed by FTIR and give recommendations for data collection. In the second part of the review, we will give examples of how synchrotron-based FTIR has been used to study the changes in secondary structure that accompany protein aggregation in neurological disease.

# IR spectroscopy: a powerful tool to study protein secondary structure

## Characterization of the secondary structure of proteins and of amyloid fibrils by FTIR

IR spectroscopy is one of the techniques used for determining the secondary structure of proteins (Susi and Byler 1987, Jackson and Mantsch 1995, Barth 2007). The peptide bond gives IR absorption peaks (Table 1) at different frequencies depending on the values of the $\psi$ and $\varphi$ angles of the neighboring molecular bonds. $\alpha$-helices, $\beta$-sheets, random coils, turns, and $3_{10}$ helices give rise to peaks at slightly different frequencies (Table 2). The amide-I peak arising mainly from the C=O stretching vibration, coupled with the N-H deformation, is considered the most informative due to the high dynamic dipole moment of this functional group. The amide-I peak of a protein backbone is broad: It represents the addition of the bands produced by the various secondary structures of the biological material. By deconvoluting the amide-I peak in its multiple contributions, it is possible to estimate the amount of the secondary structures of a protein. Assignments of peak positions are known from theoretical calculations and from correlations with X-ray diffraction data (Byler and Susi 1986, Susi and Byler 1987).

The advantages of IR spectroscopy lie in its simplicity and its versatility (Goormaghtigh et al. 2009). It is possible to assess the conformation of proteins in solution at micromolar concentrations, whether the proteins are in a dried state (Souillac et al. 2002, Hiramatsu et al. 2004), in monolayers (Roach et al. 2005, Vallée et al. 2011), in membranes (Goormaghtigh et al. 1999, Haris 2013), in microsized samples (Hiramatsu et al. 2004), in dried tissues (Rak et al. 2007), or in living cells (Miller and Dumas 2010). IR spectroscopy will also monitor conformational changes in time resolved experiments with microsecond resolution (Fabian and Naumann 2004). By coupling a spectrometer and an IR microscope equipped with a sensitive mercury cadmium telluride detector, it is possible to reduce the IR

**Table 1** IR peaks of peptide bond.

| Frequency/wavelength | Vibration type | Name | Note |
|---|---|---|---|
| 3300 $cm^{-1}$/3 μm | N-H stretching | Amide A | Insensitive to backbone conformation<br>Sensitive to hydrogen bonding |
| 3030–3100 $cm^{-1}$/3.3–3.2 μm | N-H Fermi resonance | Amide B | Resonance between amide A and an amide-II overtone |
| 1650 $cm^{-1}$/6 μm | C=O stretching (with contribution from N-H and C-N deformation) | Amide I | Very sensitive to backbone conformation |
| 1550 $cm^{-1}$/6.5 μm | N-H bending (with contribution from C-N, C-C and C-O) | Amide II | Correlation to backbone conformation is less established |
| 1200–1400 $cm^{-1}$/8.5–7 μm | N-H bending, C-N stretching | Amide III | Weakly active, sensitive to side chain composition |
| 625–725 $cm^{-1}$/16–13.8 μm | O=C-N bending | Amide IV | |
| 640–800 $cm^{-1}$/15.6–12.5 μm | N-H bending (oop) | Amide V | |
| 535–605 $cm^{-1}$/18–16.5 μm | C=O bending (oop) | Amide VI | |
| 200 $cm^{-1}$/25 μm | Skeletal C-N torsion | Amide VII | |

For assignments of side chains peaks, see Barth (2007).

**Table 2** Correspondence between amide-I peak frequencies and secondary structure assignments.

| Frequency ($cm^{-1}$) | Assignment |
|---|---|
| 1670–1695 | β-sheet[a] |
| 1662–1686 | Turn |
| 1660–1686 | $3_{10}$ helix |
| 1648–1660 | α-helix |
| 1639–1657 | Unordered |
| 1623–1641 | β-sheet[a] |
| 1610–1630 | Intermolecular β-sheet (amyloid) |

[a]Parallel when only the 1623–1641 $cm^{-1}$ component is present and antiparallel when the 1623–1641 $cm^{-1}$ and 1670–1695 $cm^{-1}$ components are associated.

beam to a size matching that of protein aggregates found in pathological tissues such as the brain of AD patients. A spatial resolution of 30–50 μm is routinely achieved with conventional instruments. One limitation resides in the difficulty to obtain the signal-to-noise ratio necessary to discriminate the signatures of the different secondary structures at very high spatial resolutions and especially at the diffraction limit (a few microns range).

Amyloid fibrils are formed by intermolecular β-sheets. Their specific signature in the IR consists of an increase in the 1610–1630 $cm^{-1}$ range, whereas native β-sheets produce absorption peaks in the 1623–1641 $cm^{-1}$ range (Choo et al. 1996, Nilsson 2004, Zandomeneghi et al. 2004, Hiramatsu and Kitagawa 2005, Sarroukh et al. 2013). By examining the amide-I bands, it is also possible to discriminate a parallel from an antiparallel arrangement of the β-strands within the amyloid aggregate (Chirgadze and Nevskaya 1976a,b, Jackson and Mantsch 1995, Cerf et al. 2009). Antiparallel β-sheets display both a strong component at 1623–1641 $cm^{-1}$ and a weaker component at 1670–1695 $cm^{-1}$, whereas parallel β-sheets display only an elevated component at 1623–1641 $cm^{-1}$ (Table 2).

## Advantages of using FTIR combined with a synchrotron source

When using the conventional sources available in commercial instruments, it is difficult to achieve the signal-to-noise ratio required to study the amide-I peak generated by protein aggregates smaller than 30 μm (such as those of HD and PD). Synchrotron sources provide the high brilliance necessary to achieve high signal-to-noise ratios at the diffraction limit or lower (Dumas et al. 2007, Miller and Dumas 2010). A synchrotron source uses the light emitted by electrons accelerated at a relativistic speed as they are deflected by electromagnetic magnets arranged in a ring configuration. The emitted light possesses remarkable properties such as a very large frequency domain (from the terahertz to the hard X-rays), high flux, very low divergence, high brilliance (number of photons per surface unit), polarization, and partial coherence; it can be seen almost as a point source. To measure the spectral signature of small protein aggregates, it is necessary to achieve a signal-to-noise ratio in the order of 500:1–1000:1. This is possible only at beamlines of third-generation synchrotron sources (Dumas et al. 2006).

## Preparation of postmortem tissue samples for FTIR analysis and data acquisition

Frozen brain samples are cut at a thickness of 8–12 μm with a cryostat. The frozen samples are attached to the cryostat

support by coating their base with small amounts of optimal cutting temperature compound (OCT) (Choo et al. 1996). Sections are then deposited on IR-compatible substrates such as $BaF_2$ or $CaF_2$ optical windows and are air-dried. Typical amyloid aggregates (as the senile plaques in AD) are visualized by using amyloid-binding dyes: either Congo red, which is a histological dye, or a fluorescent molecule, such as Thioflavin S (Choo et al. 1996, Miller et al. 2006). Aggregates not stainable by amyloid dyes, like HD inclusions (Hoffner et al. 2002), are localized by indirect immunofluorescence using antibodies specific to the causative protein. A formalin solution (10%, neutral buffered) has to be used for fixation because formalin does not hinder IR measurements (Choo et al. 1996, André et al. 2013). A standard protocol of immunofluorescence staining can be followed except that the last wash consists of double-distilled water and precedes air-drying. Immunolabeled sections can be stored at -80°C until analysis. Because of dehydration, the final thickness of the sections is diminished by about 30% (André et al. 2013).

Spectra can be collected in reflection, transreflection, or transmission mode. Reflection and transreflection modes can induce spectral distortions that need to be corrected by appropriate algorithms such as the Kramers-Kronig, Kubelka Munk, or RMieSC algorithm (Acerbo et al. 2012). High-quality spectra are typically collected in the 4000–800 $cm^{-1}$ mid-IR range, although the amide-I band covers only the 1700–1600 $cm^{-1}$ domain. The size of the microscope aperture is first adjusted to match the size of the inclusion. IR absorption spectra are then collected in two steps: the first step is to record a background spectrum on an area of the optical windows devoid of tissue. In the second step, IR spectra are collected at discrete positions within the aggregates and the surrounding tissue. Chemical maps can also be constructed by automatically collecting a large number of spectra at regular intervals on predefined areas. Because the construction of chemical maps requires the acquisition of a considerable number of spectra, chemical mapping cannot be carried out on a large number of inclusions.

### Data analysis

Several methods are used to estimate, with different precision levels, the amounts of secondary structures. The simplest method consists of visual inspection of the spectra in the amide-I region. The presence of β-sheets is generally evident from the shoulder located at 1623–1641 $cm^{-1}$. A comparison with spectra taken on surrounding tissue can also be used in order to carry out differential spectroscopy, which consists of computing the difference between the aggregate spectrum and a matching reference spectrum from tissue without aggregate. In cases where chemical maps are generated on the inclusions and the surrounding area, an image of the relative β-sheet (amyloid) content is produced by plotting the ratio of the area of the β-sheet peak to that of the α-helix peak (see Table 2 for the wavelengths). It is also possible to deconvolute the amide-I band in its different components. Deconvolution is achieved by curve-fitting procedures with or without spectral resolution enhancement techniques such as second derivative or Fourier self-deconvolution. A multivariate statistical approach can also be taken to estimate the amount of amyloid β-sheets by comparison with a model or to classify aggregates based on the profile of their amide-I band (André et al. 2013).

IR spectra recorded with a microscope are subject to specific artefacts not observed with protein solutions. One such artefact is the Mie scattering that affects spectra recorded on spherical objects whose size is close to the IR wavelength used (6 μm in the amide-I band), such as protein aggregates and cell organelles (nucleus, nucleolus, etc.). Mie scattering is caused by a change in sample refractive index and affects the absorption properties. The resulting spectral distortions modify the amide-I band profile and can alter the estimation of the β-sheet content. Although several methods for correcting Mie scattering have been published (Mohlenhoff et al. 2005, Kohler et al. 2008, Bassan et al. 2010a,b), it is impossible to achieve exact analytical correction of each spectrum because of unknown local variations in radius, curvature, and refractive index of the sample. Thus, it is best to discard the spectra with Mie scattering. Spectra recorded in transreflection mode are particularly affected by Mie scattering; thus, transmission is the preferred mode for collecting IR spectra of protein aggregates.

## Application of synchrotron-based FTIR to the study of protein aggregates in the brain of patients with neurological disease

### Alzheimer's disease

Senile plaques are protein aggregates with a 10–160 μm diameter (50 μm on average) (Armstrong et al. 1991). These protein deposits are composed mostly of the Aβ peptide

(4 kDa), a cleavage product of the amyloid β-precursor protein (120 kDa) (Maury 1995). Based on morphology, two categories of senile plaques have been described: dense-core plaques and diffuse plaques (Yamaguchi et al. 1988). A few papers have reported the characterization of AD senile plaques by synchrotron-based FTIR. Analysis with a spatial resolution of 12 μm×12 μm of one senile plaque and one amyloid deposit within the walls of a blood vessel (cerebral angiopathy) of an AD patient revealed an increase in components at 1631 $cm^{-1}$ and ~1633 $cm^{-1}$, respectively. Both components are indicative of β-sheet structures (Choo et al. 1996). These findings were later corroborated by a thorough analysis of about 30 plaques from two AD cases (Miller et al. 2006) and by examination with a subcellular resolution of 0.54 μm×0.54 μm of senile plaques from a 91-year-old AD patient (Figure 1) (Liao et al. 2013).

Transgenic mice simulating AD have also been used to study the senile plaques of hippocampus, cortex, and caudate/putamen (Rak et al. 2007, Liao et al. 2013). TgCRND8 mice express the human amyloid precursor protein (APP) with both the Swedish K670N/M671L and Indiana V717 FAD mutations (Chishti et al. 2001). The triply transgenic 3xTg mice express the KM670/671NL mutation in APP, the presenilin mutation PS1 (M146V), and the P310L mutation in human four-repeat Tau (Oddo et al. 2003). Several tens of dense core and diffuse plaques were examined at early and late stages of formation in TgCRND8 and 3xTg mice. Dense-core congophilic senile plaques displayed an amide-I maximum at 1623 $cm^{-1}$ but no increase in higher-frequency bands at 1680–1690 $cm^{-1}$. This indicated a parallel β-sheet structure (Figure 1). In contrast, noncongophilic diffuse plaques showed no alterations in protein secondary structure. Therefore, although both mouse and human dense-core senile plaques share an enrichment in amyloid β-sheets, the two species differ in their amide-I maximum: 1631–1633 $cm^{-1}$ in human AD brain and 1623 $cm^{-1}$ in transgenic mice (Choo et al. 1996, Rak et al. 2007). It may be concluded that the structural arrangement of the Aβ fibrils inside the plaques differs in transgenic mice and patients.

Aggregation of synthetic Aβ is, like htt peptide aggregation, modulated by experimental conditions such as pH, temperature, solvent, and physicochemical nature of the surface (Kowalewski and Holtzman 1999, Huang et al. 2000, Nichols et al. 2005). Aβ polymorphic amyloid aggregates with an amide-I maximum in the 1620–1628 $cm^{-1}$ range and amorphous aggregates with no regular secondary structure can be formed. Based on the amide-I maximum, the structure of dense-core plaques produced in transgenic mice appears to resemble more closely that

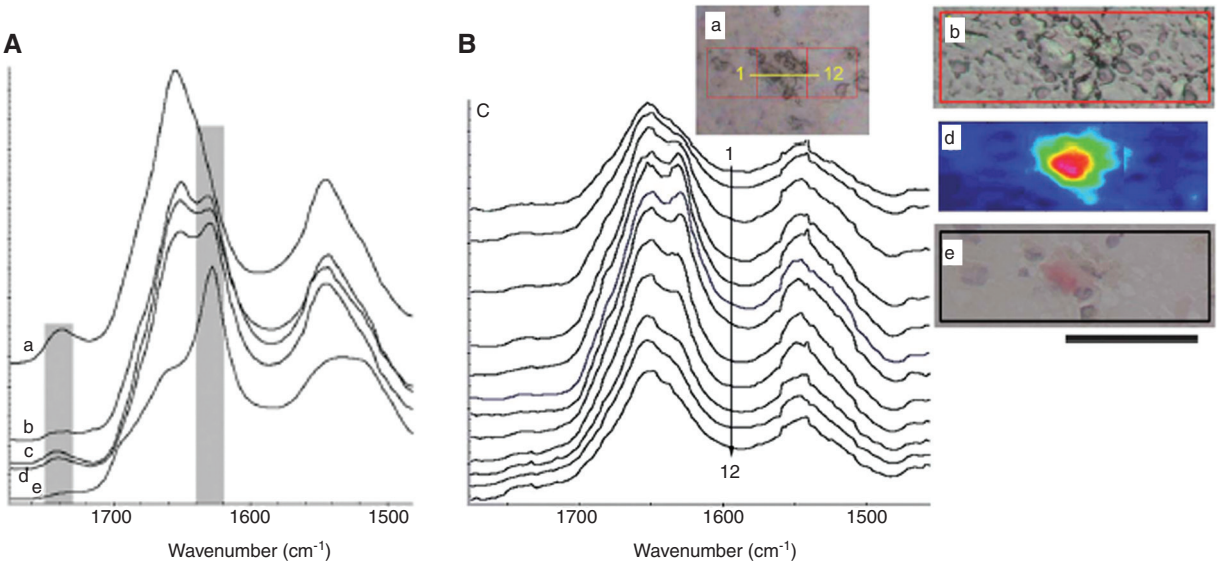



**Figure 1** Synchrotron-FTIR analysis of senile plaques in human and transgenic mouse AD brain. (A) Amide-I and -II regions from (a) mouse grey matter, (b) human plaque core, (c) TgCRND8 mouse plaque core, (d) 3xTg mouse plaque core, and (e) fibrillar Aβ42. The CO stretch peak and the β-sheet peak in the amide-I band are highlighted with a gray box. With the exception of (e), spectra are displayed on a common scale, offset for clarity. (B) Amide-I and -II regions and images of dense core hippocampus plaque from a 91-year-old AD patient. (a) Images viewed through FTIR microscope. (b) Images viewed through light microscope. (c) Stack of 12 spectra spanning the plaque and extracted from image along yellow line in (a). (d) False-color images of the 3×1 tile mosaic treated to show amide-I band intensity due to β-sheet. Color indicates low (blue) to high (red) content in β-sheet. (e) Photograph of tissue stained after FTIR imaging: plaque core is stained red by Congo red and nuclei blue by hematoxylin. Scale bar, 50 μm. Reproduced and adapted from Liao et al. (2013).

of Aβ fibrils formed *in vitro* than those of AD brain (Lansbury 1992, Fabian et al. 1993, Choo et al. 1996, Miller et al. 2006, Rak et al. 2007, Liao et al. 2013, Shivu et al. 2013).

To our knowledge, the characterization of senile plaques associated with familial AD has not been reported. It would be interesting to investigate the structure of these senile plaques (dense-cored and diffuse) in order to determine if they differ from those of late-onset AD. Examination of the senile plaques that form in other neurologic diseases, such as trisomy 21 or senile dementia, or even during normal aging may also be relevant.

## Parkinson's disease

Lewy bodies are 5–25 μm in diameter and are localized in the nerve cell bodies of neurons. We know of only one report on the use of synchrotron-based FTIR to study protein structure in PD neurons (Szczerbowska-Boruchowska et al. 2007). In this study, four neurons of the substantia nigra of a single PD patient were compared with three neurons of each of four control cases. Examination of spectra and of their second derivatives revealed that the amide-I maximum was somewhat shifted to higher frequencies in PD neurons (from 1656 $cm^{-1}$ to 1662 $cm^{-1}$). In addition, two new peaks were detected at 1643 $cm^{-1}$ and 1682 $cm^{-1}$. The authors assigned the 1643 $cm^{-1}$ and 1682 $cm^{-1}$ frequencies to β-sheets and β-turns, respectively. The structural changes observed in PD substantia nigra probably reflect the accumulation of misfolded and aggregated α-synuclein in neuronal bodies. A thorough investigation of the structure of Lewy bodies awaits to be done. Comparison of the Lewy bodies found in the various α-synucleopathies may bring valuable information about overlaps and distinctive features of the members of this group of diseases.

## Prion diseases

Analysis by FTIR spectroscopy of $PrP^{c}$ and $PrP^{Sc}$ purified from the brain of scrapie-infected hamsters and uninfected controls has demonstrated that the β-sheet content of $PrP^{Sc}$ is nearly 15 times higher than that of $PrP^{c}$ (Pan et al. 1993). Because $PrP^{Sc}$ represents as little as 0.1% of total brain proteins, direct detection of structural changes in infected tissue requires the use of FTIR coupled to a synchrotron source (Kneipp et al. 2003). The group of Dieter Naumann and Lisa Miller has particularly contributed to the study of prion aggregation by synchrotron-based FTIR. They have examined the dorsal root ganglia of hamsters orally infected with scrapie (Kneipp et al. 2003, Wang et al. 2005, Kretlow et al. 2006, 2008). Comparison of spectra derived from neurons of infected animals with those of uninfected animals showed a decrease in α-helical content and an increase in β-sheet content in some neurons of infected animals. Analysis of second derivatives demonstrated that the β-sheet enrichment was due to increases in the peaks at ~1637 $cm^{-1}$ and 1625–1632 $cm^{-1}$. Comparison of sections stained for $PrP^{Sc}$ with IR images showed a correlation between increased β-sheet content and intense PrP staining (Kneipp et al. 2003). The consistency of the spectral differences between infected and normal tissue has suggested that FTIR microspectroscopy could detect $PrP^{Sc}$ without the necessity of immunostaining. This would open the way to spectroscopy-based TSE detection (Kretlow et al. 2006).

In another study, protein structure changes during disease progression in infected hamsters were examined by synchrotron-based FTIR (at preclinical stages, first clinical signs, and terminal stage). An increase in β-sheet content was detected already at preclinical stages (Figure 2). As an elevated β-sheet content did not always spatially correspond to a strong PrP staining at the terminal stage, the authors proposed that β-sheet-rich proteins other than $PrP^{Sc}$ were overproduced during the course of the disease (Kretlow et al. 2008).

Investigation by FTIR of the structure of four TSE strains adapted to Syrian hamster (263 K, 22A-H, ME7-H, and BSE-H) has shown that these strains possess discriminative IR features (Thomzig et al. 2004). While all four TSE strains display an elevated peak at 1620 $cm^{-1}$, they differ by the elevation of another peak in the 1630–1637 $cm^{-1}$ range. A synchrotron-based FTIR analysis of $PrP^{Sc}$ protein aggregates in the brain of human patients remains to be done. Analysis of the $PrP^{Sc}$ protein aggregates that develop in Gerstmann-Straüssler-Scheinker syndrome, Kuru, fatal familial insomnia, CJD, and variant CJD might reveal differences between the structures of the TSE agents responsible for these various diseases and might be of diagnostic value.

## ALS

Like in the other neurological diseases with protein aggregation, the SOD1 aggregates found in hereditary ALS are detergent-insoluble. Aggregated SOD1 consists of unmodified enzyme lacking both posttranslational modifications and metallation (Shaw et al. 2008). It has been shown by FTIR spectroscopy, using the pure protein, that removal of copper and zinc ions, reduction of disulfide bridges, and familial ALS mutations all promoted the formation of aggregates with high β-sheet content (Oztug Durer et al.

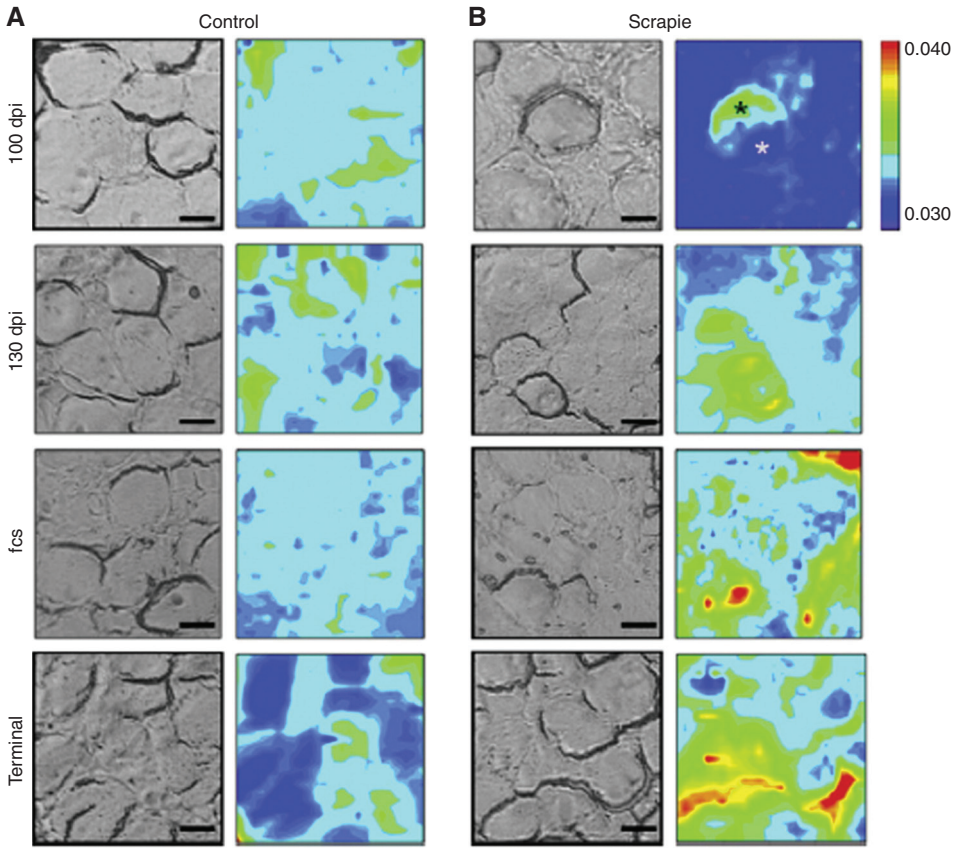



**Figure 2** Synchrotron-FTIR analysis of prion disease. Chemical maps showing the β-sheet content in ganglia of Syrian hamster during scrapie progression. Ganglia from uninfected controls (A) and infected (B) hamsters are illustrated. Images of unlabeled frozen sections (left panels) and corresponding chemical maps showing the β-sheet/α-helix ratio (right panels) were obtained at 100 and 130 days post infection (dpi), at time of first clinical signs (fcs), and at terminal stage. The β-sheet/α-helix ratio is represented by a color scale going from red (highest) to blue (lowest or nil). Scale bar, 20 μm. Reproduced and adapted from Kretlow et al. (2008). White asterisk shows that at 100 dpi spectrum is essentially α-helical in most cells; black asterisk identifies area near cell membrane with higher β-sheet content.

2009). In one study, the structure of aggregated mutant SOD1 was studied by synchrotron-based FTIR. The aggregates were formed in cultured cells transfected with an expression vector encoding the mutant enzyme fused to the yellow fluorescent protein. Time-lapsed FTIR imaging showed a shift of the amide-I band to higher frequencies, suggesting an increase in the amount of antiparallel β-sheets (Miller et al. 2013).

## Huntington's disease

The first use of synchrotron-based FTIR in the study of htt aggregation was carried out in rats simulating HD. The authors injected the right striatum of rats with a lentivirus encoding a mutant htt fragment with $Q_{82}$, while the left striatum was injected with a construct encoding a normal-length htt fragment. β-sheet enrichment was detected in the right striatum, but not in the left striatum, as early as 4 weeks after injection. No spatial correlation was established between aggregate formation and β-sheet enrichment (Bonda et al. 2011).

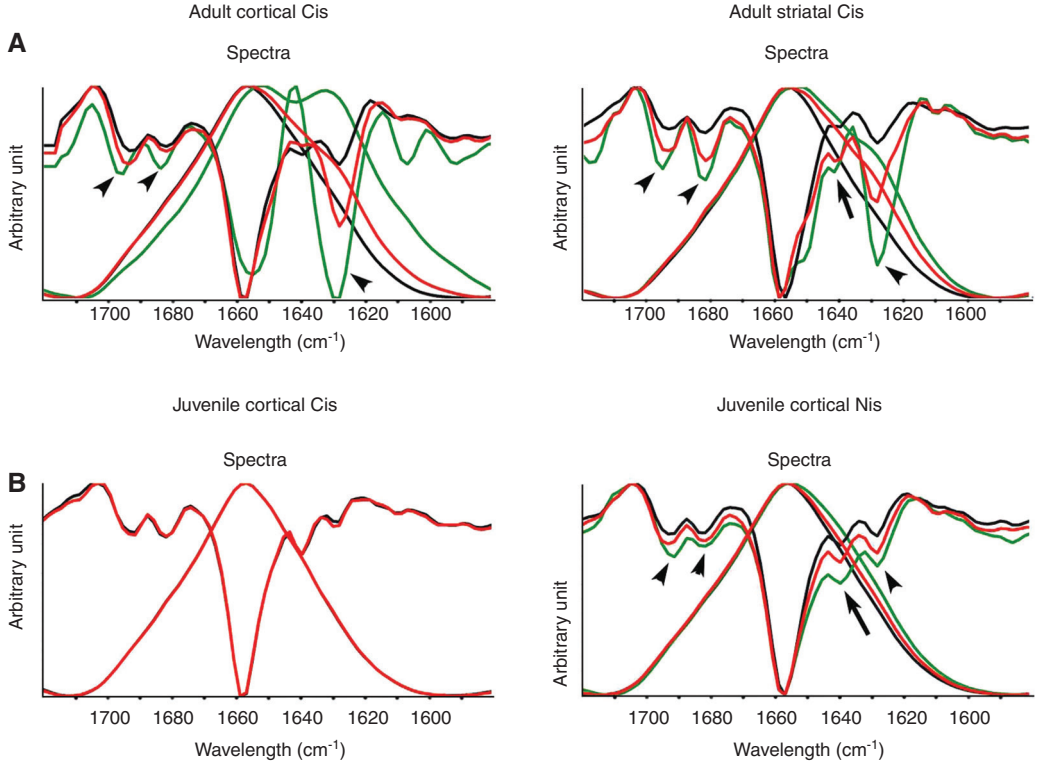
Our group provided the first report of the secondary structure of proteins aggregated in the brain of patients with Huntington's disease (André et al. 2013). By combining a synchrotron source with an IR microscope, we were able to reach the high sensitivity and high spatial resolution (6×6 $\mu m^2$) required for probing the inclusions of patients. Measurements were carried out at the IR beamline (SMIS) of the SOLEIL synchrotron in Saint-Aubin, France. Inclusions were first visualized by immunological staining using an anti-N-terminal htt antibody. High-quality IR spectra were collected in the mid-IR range (4000–800 $cm^{-1}$), and the secondary structure of proteins was addressed by analyzing the amide-I band. Spectra were screened for Mie scattering by using five parameters: sine shape of the baseline, shape of the ester C=O peak at 1740 $cm^{-1}$, position of the amide-I band, height of the

1515 $cm^{-1}$ amide-II shoulder, and width of the separation between the amide II and CH deformation peak at 1460 $cm^{-1}$. Statistical analysis was performed not only on the original spectra but also on their second derivatives as these increase the discriminative features present in the original spectra. We used principal component analysis, a multivariate data analysis that highlights the principal components causing the differences between groups of spectra. As the width of the amide-I band varied between patients, we did not attempt interindividual comparisons, but instead favored intraindividual analyses, in which we compared the inclusions with their surrounding tissue.

We first studied cortical and striatal inclusions of adult patients (Figure 3A). Both cortical and striatal cytoplasmic inclusions (Cis) of AHD patients shared an amyloid structure since they showed a higher intensity of the 1627 $cm^{-1}$ peak. These inclusions also shared an increase in the 1693 $cm^{-1}$ peak, which, like the 1627 $cm^{-1}$ peak, is characteristic of β-sheets (Table 2). However, the AHD Cis of striatum differed from those of cortex by a higher contribution of the 1639 $cm^{-1}$ peak. As shown in Table 2, the assignment of the 1639 $cm^{-1}$ was ambiguous, as this wavelength is at the boundary between β-sheet and unordered structures. Therefore, we attributed the 1639 $cm^{-1}$ peak to "unordered/β-sheet" structures. We then studied the inclusions of juvenile patients (Figure 3B). JHD Cis did not show any detectable structural rearrangement. As to JHD nuclear inclusions (Nis), their spectra presented an elevation of the contribution of the 1627, 1693, and 1639 $cm^{-1}$ peaks. Therefore, JHD Nis had a structural IR signature closely resembling that of striatal AHD Cis.

We attempted to determine whether the β-strands in the inclusions were parallel or antiparallel (Chirgadze and Nevskaya 1976a,b, Cerf et al. 2009). An increase in the antiparallel β-sheet/α-helix ratio suggested that AHD Cis and JHD Nis contained high levels of antiparallel β-sheets. Reduction of the antiparallel β-sheet/total β-sheet ratio in these inclusions also indirectly suggested enrichment in parallel β-sheets. As this ratio was lower in AHD Cis than in JHD Nis, AHD Cis might be richer than JHD Nis in parallel β-sheets. We concluded that amyloid inclusions of HD brain, whether juvenile, adult, nuclear, or cytoplasmic, comprise both parallel and antiparallel β-sheets.

We noticed that the contribution of β-sheet structures was more or less marked within a given patient. This could have resulted from variations in inclusion size, as a greater proportion of the surrounding inclusion-free tissue would be included when analyzing small inclusions than when analyzing larger ones. A comparison between the size of the inclusions and their relative absorbance at 1627 $cm^{-1}$ demonstrated that β-sheet enrichment was not related to inclusion size and therefore presumably reflected genuine




(**Figure 3** Continued)

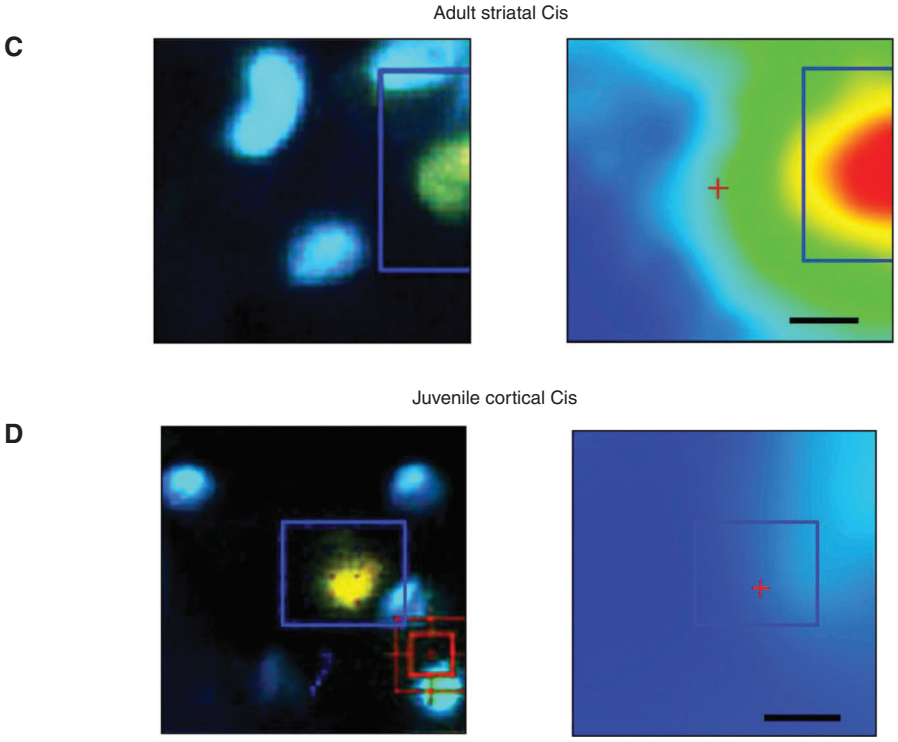



**Figure 3** Synchrotron-FTIR analysis of inclusions in Huntington's disease brain. (A) IR analyses of cortical Cis of one representative adult case and of striatal Cis of another representative adult case are illustrated. Spectra of Cis are compared to spectra of cytoplasm. Average spectra of Cis (red) and cytoplasm (black), spectra of Cis most divergent from cytoplasm (green), and corresponding secondary spectra (with same colors) are displayed. (B) IR analyses of cortical Cis of one juvenile patient and of Nis of another juvenile patient are illustrated. Spectra of Nis are compared to spectra of nuclei; analysis is performed as in (A). Arrowheads mark enrichments in peaks assigned to β-sheets at 1627 $cm^{-1}$, 1681 $cm^{-1}$, and 1693 $cm^{-1}$. The peak at 1627 $cm^{-1}$ indicates the amyloid nature of adult Cis and juvenile Nis; absence of this peak in juvenile Cis shows their nonamyloid nature. Arrows in striatal adult Cis and cortical juvenile Nis reveal additional contribution of a peak assigned to β-sheet/unordered structure at 1639 $cm^{-1}$. Therefore adult Cis and juvenile Nis possess amyloid structures with distinct characteristics (a component at 1639 $cm^{-1}$). (C) Chemical map of β-sheet content of an adult striatal Cis. (Left panel) Fluorescent labeling of Cis (green) and nuclei (blue). (Right panel) β-sheet/α-helix ratio displayed by color scale going from red (highest) to blue (lowest or nil). Correspondence between inclusion and area with highest β-sheet content is obvious. (D) Chemical map of β-sheet content of cortical juvenile Cis. (Left panel) Fluorescent labeling of Cis (yellow) and nuclei (blue). (Right panel) β-sheet/α-helix ratio. No increase in β-sheet content is observed in inclusion. Scale bars: 2 μm. (A), (B), and (C) reproduced and adapted from André et al. (2013).

secondary structure variability. Chemical maps representing the β-sheet/α-helix ratio of inclusions confirmed that striatal AHD Cis were amyloid (Figure 3C), whereas JHD Cis did not have a particular structure when compared to the surrounding cytoplasm (Figure 3D).

Microscopic aggregates are thought to assemble from submicroscopic aggregates such as oligomers and protofibrils. These forms of aggregation would be detected as structural abnormalities located outside the inclusions and would be expected to partition in the same way as inclusions do: nuclear in JHD and cytoplasmic in AHD. We indeed detected an elevation in the β-sheet content (in an antiparallel configuration) of the nuclei but not the cytoplasm of one JHD case and of the cytoplasm but not the nuclei of an AHD case. This suggested the presence of oligomers with an antiparallel β-sheet structure.

In conclusion, we demonstrated that the secondary structure of the aggregated proteins varied according to the brain region and the type of disease (juvenile or adult). We hypothesize that the length of the polyQ as well as factors specific to subcellular compartment and/or brain region modulate aggregation and explain why inclusions are structurally polymorphic. The structural polymorphism of htt inclusions that we have observed using FTIR may reconcile the seemingly opposite views on inclusion toxicity (Saudou et al. 1998, Hoffner and Djian 2002, Arrasate et al. 2004). Amyloid inclusions with a β-sheet/unordered component at 1639 $cm^{-1}$ are characteristic of the brain regions most affected by HD, whereas inclusions lacking the 1639 $cm^{-1}$ component, whether amyloid or not, are found in less affected brain regions. Therefore, it appears that the highest neuronal toxicity is

specifically related to amyloid aggregates with a 1639 $cm^{-1}$ component.

## Conclusion

In this review, we have given the reasons for which FTIR combined with synchrotron radiation is a powerful technique for probing the structure of the protein aggregates that form in neurological diseases. Although the evidence is still scanty, studies by synchrotron-based FTIR carried out in human brain have already produced results supporting the view that neuronal aggregates are structurally diverse and that their structure determines their toxicity. Defining the toxic conformations is necessary in order to understand how the protein aggregates cause neuronal death in this particularly devastating group of human diseases.

**Acknowledgments:** We are grateful to CNRS, INSERM, the SOLEIL synchrotron, and Université Paris Descartes for financial support.

## References

Acerbo, A. S.; Carr, G. L.; Judex, S.; Miller, L. M. Imaging the material properties of bone specimens using reflection-based infrared microspectroscopy. *Anal. Chem*. **2012**, *84*, 3607–3613.

André, W.; Sandt, C.; Dumas, P.; Djian, P.; Hoffner, G. Structure of inclusions of Huntington's disease brain revealed by synchrotron infrared microspectroscopy: polymorphism and relevance to cytotoxicity. *Anal. Chem*. **2013**, *85*, 3765–3773.

Armstrong, R. A.; Myers, D.; Smith, C. U. Alzheimer's disease: size class frequency distribution of senile plaques: do they indicate when a brain tissue was affected? *Neurosci. Lett*. **1991**, *127*, 223–226.

Arrasate, M.; Mitra, S.; Schweitzer, E.; Segal, M.; Finkbeiner, S. Inclusion body formation reduces levels of mutant huntingtin and the risk of neuronal death. *Nature* **2004**, *431*, 805–810.

Barth, A. Infrared spectroscopy of proteins. *Biochim. Biophys. Acta* **2007**, *1767*, 1073–1101.

Bassan, P.; Kohler, A.; Martens, H.; Lee, J.; Byrne, H. J.; Dumas, P.; Gazi, E.; Brown, M.; Clarke, N.; Gardner, P. Resonant Mie scattering (RmieS) correction of infrared spectra from highly scattering biological samples. *Analyst* **2010a**, *135*, 268–277.

Bassan, P.; Kohler, A.; Martens, H.; Lee, J.; Jackson, E.; Lockyer, N.; Dumas, P.; Brown, M.; Clarke, N.; Gardner, P. RMieS-EMSC correction for infrared spectra of biological cells: extension using full Mie theory and GPU computing. *J. Biophotonics* **2010b**, *3*, 609–620.

Bonda, M.; Perrin, V.; Vileno, B.; Runne, H.; Kretlow, A.; Forró, L.; Luthi-Carter, R.; Miller, L. M.; Jeney, S. Synchrotron infrared microspectroscopy detecting the evolution of Huntington's disease neuropathology and suggesting unique correlates of dysfunction in white *versus* gray brain matter. *Anal. Chem*. **2011**, *83*, 7712–7720.

Bruijn, L. I.; Becher, M. W.; Lee, M. K.; Anderson, K. L.; Jenkins, N. A.; Copeland, N. G.; Sisodia, S. S.; Rothstein, J. D.; Borchelt, D. R.; Price, D. L.; Cleveland, D. W. ALS-linked SOD1 mutant G85R mediates damage to astrocytes and promotes rapidly progressive disease with SOD1-containing inclusions. *Neuron* **1997**, *18*, 327–338.

Byler, D. M.; Susi, H. Examination of the secondary structure of proteins by deconvolved FTIR spectra. *Biopolymers* **1986**, *25*, 469–487.

Cerf, E.; Sarroukh, R.; Tamamizu-Kato, S.; Breydo, L.; Derclaye, S.; Dufrêne, Y. F.; Narayanaswami, V.; Goormaghtigh, E.; Ruysschaert, J. M.; Raussens, V. Antiparallel beta-sheet: a signature structure of the oligomeric amyloid beta-peptide. *Biochem. J*. **2009**, *421*, 415–423.

Chirgadze, Y. N.; Nevskaya, N. A. Infrared spectra and resonance interaction of amide-I vibration of the antiparallel-chain pleated sheet. *Biopolymers* **1976a**, *15*, 607–625.

Chirgadze, Y. N.; Nevskaya, N. A. Infrared spectra and resonance interaction of amide-I vibration of the parallel-chain pleated sheets. *Biopolymers* **1976b**, *15*, 627–636.

Chishti, M. A.; Yang, D. S.; Janus, C.; Phinney, A. L.; Horne, P.; Pearson, J.; Strome, R.; Zuker, N.; Loukides, J.; French, J.; Turner, S.; Lozza, G.; Grilli, M.; Kunicki, S.; Morissette, C.; Paquette, J.; Gervais, F.; Bergeron, C.; Fraser, P. E.; Carlson, G. A.; George-Hyslop, P. S.; Westaway, D. Early-onset amyloid deposition and cognitive deficits in transgenic mice expressing a double mutant form of amyloid precursor protein 695. *J. Biol. Chem*. **2001**, *276*, 21562–21570.

Choo, L. P.; Wetzel, D. L.; Halliday, W. C.; Jackson, M.; LeVine, S. M.; Mantsch, H. H. In situ characterization of beta-amyloid in Alzheimer's diseased tissue by synchrotron Fourier transform infrared microspectroscopy. *Biophys. J*. **1996**, *71*, 1672–1679.

Delacourte, A.; Défossez, A. Biochemical characterization of an immune serum which specifically marks neurons in neurofibrillary degeneration in Alzheimer's disease. *C R Acad. Sci. III* **1986**, *303*, 439–444.

DiFiglia, M.; Sapp, E.; Chase, K. O.; Davies, S. W.; Bates, G. P.; Vonsattel, J. P.; Aronin, N. Aggregation of huntingtin in neuronal intranuclear inclusions and dystrophic neurites in brain. *Science* **1997**, *277*, 1990–1993.

Dumas, P.; Polack, F.; Lagarde, B.; Chubar, O.; Giogetta, J. L.; Lefrançois, S. Synchrotron infrared microscopy at the French Synchrotron Facility SOLEIL. *Infrared Phys. Technol*. **2006**, *49*, 152–160.

Dumas, P.; Sockalingum, G. D.; Sulé-Suso, J. Adding synchrotron radiation to infrared microspectroscopy: what's new in biomedical applications? *Trends Biotechnol*. **2007**, *25*, 40–44.

Fabian, H.; Naumann, D. Methods to study protein folding by stopped-flow FT-IR. *Methods* **2004**, *34*, 28–40.

Fabian, H.; Choo, L.-P.; Szendrei, G.; Jackson, M.; Halliday, W.; Otvos, L.; Mantsch, H. Infrared spectroscopic characterization of Alzheimer plaques. *Appl. Spectrosc*. **1993**, *47*, 1513–1518.

Fändrich, M. On the structural definition of amyloid fibrils and other polypeptide aggregates. *Cell. Mol. Life Sci*. **2007**, *64*, 2066–2078.

Goedert, M.; Spillantini, M. G. Lewy body diseases and multiple system atrophy as alpha-synucleinopathies. *Mol. Psychiatry* **1998**, *3*, 462–465.

Goormaghtigh, E.; Raussens, V.; Ruysschaert, J. M. Attenuated total reflection infrared spectroscopy of proteins and lipids in biological membranes. *Biochim. Biophys. Acta* **1999**, *1422*, 105–185.

Goormaghtigh, E.; Gasper, R.; Bénard, A.; Goldsztein, A.; Raussens V. Protein secondary structure content in solution, films and tissues: redundancy and complementarity of the information content in circular dichroism, transmission and ATR FTIR spectra. *Biochim. Biophys. Acta* **2009**, *1794*, 1332–1343.

Grundke-Iqbal, I.; Iqbal, K.; Tung, Y. C.; Quinlan, M.; Wisniewski, H. M.; Binder, L. I. Abnormal phosphorylation of the microtubule-associated protein tau (tau) in Alzheimer cytoskeletal pathology. *Proc. Natl. Acad. Sci. USA* **1986**, *83*, 4913–4917.

Haris, P. I. Probing protein-protein interaction in biomembranes using Fourier transform infrared spectroscopy. *Biochim. Biophys. Acta* **2013**, *1828*, 2265–2271.

Hiramatsu, H.; Kitagawa, T. FT-IR approaches on amyloid fibril structure. *Biochim. Biophys. Acta* **2005**, *1753*, 100–107.

Hiramatsu, H.; Goto, Y.; Naiki, H.; Kitagawa, T. Core structure of amyloid fibril proposed from IR-microscope linear dichroism. *J. Am. Chem. Soc*. **2004**, *126*, 3008–3009.

Hirsch, T. Z.; Hernandez-Rapp, J.; Martin-Lannerée, S.; Launay, J. M.; Mouillet-Richard, S. PrP(C) signalling in neurons: from basics to clinical challenges. *Biochimie* **2014**, *104C*, 2–11.

Hoffner, G.; Djian, P. Protein aggregation in Huntington's disease. *Biochimie* **2002**, *84*, 273–278.

Hoffner, G.; Djian, P. Monomeric, oligomeric and polymeric proteins in Huntington disease and other diseases of polyglutamine expansion. *Brain Sci*. **2014**, *4*, 91–122.

Hoffner, G.; Kahlem, P.; Djian, P. Perinuclear localization of huntingtin as a consequence of its binding to microtubules through an interaction with beta-tubulin: relevance to Huntington's disease. *J. Cell Sci*. **2002**, *115*, 941–948.

Hoffner, G.; Island, M.; Djian, P. Purification of neuronal inclusions of patients with Huntington's disease reveals a broad range of N-terminal fragments of expanded huntingtin and insoluble polymers. *J. Neurochem*. **2005**, *95*, 125–136.

Huang, T. H.; Yang, D. S.; Plaskos, N. P.; Go, S.; Yip, C. M.; Fraser, P. E.; Chakrabartty, A. Structural studies of soluble oligomers of the Alzheimer beta-amyloid peptide. *J. Mol. Biol*. **2000**, *297*, 73–87.

Jackson, M.; Mantsch, H. H. The use and misuse of FTIR spectroscopy in the determination of protein structure. *Crit. Rev. Biochem. Mol. Biol*. **1995**, *30*, 95–120.

Kang, J.; Lemaire, H. G.; Unterbeck, A.; Salbaum, J. M.; Masters, C. L.; Grzeschik, K. H.; Multhaup, G.; Beyreuther, K.; Müller-Hill, B. The precursor of Alzheimer's disease amyloid A4 protein resembles a cell-surface receptor. *Nature* **1987**, *325*, 733–736.

Kneipp, J.; Miller, L. M.; Joncic, M.; Kittel, M.; Lasch, P.; Beekes, M.; Naumann, D. In situ identification of protein structural changes in prion-infected tissue. *Biochim. Biophys. Acta* **2003**, *1639*, 152–158.

Kohler, A.; Sulé-Suso, J.; Sockalingum, G. D.; Tobin, M.; Bahrami, F.; Yang, Y.; Pijanka, J.; Dumas, P.; Cotte, M.; van Pittius, D. G.; Parkes, G.; Martens, H. Estimating and correcting mie scattering in synchrotron-based microscopic Fourier transform infrared spectra by extended multiplicative signal correction. *Appl. Spectrosc*. **2008**, *62*, 259–266.

Kosik, K. S.; Joachim, C. L.; Selkoe, D. J. Microtubule-associated protein tau (tau) is a major antigenic component of paired helical filaments in Alzheimer disease. *Proc. Natl. Acad. Sci. USA* **1986**, *83*, 4044–4048.

Kowalewski, T.; Holtzman, D. M. In situ atomic force microscopy study of Alzheimer's beta-amyloid peptide on different substrates: new insights into mechanism of beta-sheet formation. *Proc. Natl. Acad. Sci. USA* **1999**, *96*, 3688–3693.

Kretlow, A.; Wang, Q.; Kneipp, J.; Lasch, P.; Beekes, M.; Miller, L.; Naumann, D. FTIR-microspectroscopy of prion-infected nervous tissue. *Biochim. Biophys. Acta* **2006**, *1758*, 948–959.

Kretlow, A.; Wang, Q.; Beekes, M.; Naumann, D.; Miller, L. M. Changes in protein structure and distribution observed at preclinical stages of scrapie pathogenesis. *Biochim. Biophys. Acta* **2008**, *1782*, 559–565.

Landles, C.; Sathasivam, K.; Weiss, A.; Woodman, B.; Moffitt, H.; Finkbeiner, S.; Sun, B.; Gafni, J.; Ellerby, L. M.; Trottier, Y.; Richards, W. G.; Osmand, A.; Paganetti, P.; Bates, G. P. Proteolysis of mutant huntingtin produces an exon 1 fragment that accumulates as an aggregated protein in neuronal nuclei in Huntington disease. *J. Biol. Chem*. **2010**, *285*, 8808–8823.

Lansbury, P. T. In pursuit of the molecular structure of amyloid plaque, new technology provides unexpected and critical information. *Biochemistry* **1992**, *31*, 6865–6870.

Lennox, G.; Lowe, J.; Morrell, K.; Landon, M.; Mayer, R. J. Anti-ubiquitin immunocytochemistry is more sensitive than conventional techniques in the detection of diffuse Lewy body disease. *J. Neurol. Neurosurg. Psychiatry* **1989**, *52*, 67–71.

Lewy, F. H. Paralysis agitans. 1. Pathologische anatomie. In Handbuch der Neurologie. Lewandowsky, M., editor. Julius Springer: Berlin, 1912; Vol 3, pp 920–933.

Liao, C. R.; Rak, M.; Lund, J.; Unger, M.; Platt, E.; Albensi, B. C.; Hirschmugl, C. J.; Gough, K. M. Synchrotron FTIR reveals lipid around and within amyloid plaques in transgenic mice and Alzheimer's disease brain. *Analyst* **2013**, *138*, 3991–3997.

Maury, C. P. Molecular pathogenesis of beta-amyloidosis in Alzheimer's disease and other cerebral amyloidoses. *Lab. Invest*. **1995**, *72*, 4–16.

Miller, L. M.; Dumas, P. From structure to cellular mechanism with infrared microspectroscopy. *Curr. Opin. Struct. Biol*. **2010**, *20*, 649–656.

Miller, L.; Wang, Q.; Telivala, T.; Smith, R.; Lanzirotti, A.; Miklossy, J. Synchrotron-based infrared and X-ray imaging shows focalized accumulation of Cu and Zn co-localized with beta-amyloid deposits in Alzheimer's disease. *J. Struct. Biol*. **2006**, *155*, 30–37.

Miller, L. M.; Bourassa, M. W.; Smith, R. J. FTIR spectroscopic imaging of protein aggregation in living cells. *Biochim. Biophys. Acta* **2013**, *1828*, 2339–2346.

Mohlenhoff, B.; Romeo, M.; Diem, M.; Wood, B. R. Mie-type scattering and non-Beer-Lambert absorption behavior of human cells in infrared microspectroscopy. *Biophys. J*. **2005**, *88*, 3635–3640.

Nekooki-Machida, Y.; Kurosawa, M.; Nukina, N.; Ito, K.; Oda, T.; Tanaka, M. Distinct conformations of *in vitro* and *in vivo* amyloids of huntingtin-exon1 show different cytotoxicity. *Proc. Natl. Acad. Sci. USA* **2009**, *106*, 9679–9684.

Nichols, M. R.; Moss, M. A.; Reed, D. K.; Hoh, J. H.; Rosenberry, T. L. Rapid assembly of amyloid-beta peptide at a liquid/liquid interface produces unstable beta-sheet fibers. *Biochemistry* **2005**, *44*, 165–173.

Nilsson, M. R. Techniques to study amyloid fibril formation *in vitro*. *Methods* **2004**, *34*, 151–160.

Oddo, S.; Caccamo, A.; Kitazawa, M.; Tseng, B. P.; LaFerla, F. M. Amyloid deposition precedes tangle formation in a triple transgenic model of Alzheimer's disease. *Neurobiol. Aging* **2003**, *24*, 1063–1070.

Oztug Durer, Z. A.; Cohlberg, J. A.; Dinh, P.; Padua, S.; Ehrenclou, K.; Downes, S.; Tan, J. K.; Nakano, Y.; Bowman, C. J.; Hoskins, J. L.; Kwon, C.; Mason, A. Z.; Rodriguez, J. A.; Doucette, P. A.; Shaw, B. F.; Valentine, J. S. Loss of metal ions, disulfide reduction and mutations related to familial ALS promote formation of amyloid-like aggregates from superoxide dismutase. *PLoS One* **2009**, *4*, e5004.

Pan, K. M.; Baldwin, M.; Nguyen, J.; Gasset, M.; Serban, A.; Groth, D.; Mehlhorn, I.; Huang, Z.; Fletterick, R. J.; Cohen, F. E. Conversion of alpha-helices into beta-sheets features in the formation of the scrapie prion proteins. *Proc. Natl. Acad. Sci. USA* **1993**, *90*, 10962–10966.

Prusiner, S. B. Novel proteinaceous infectious particles cause scrapie. *Science* **1982**, *216*, 136–144.

Rak, M.; Del Bigio, M. R.; Mai, S.; Westaway, D.; Gough, K. Dense-core and diffuse Abeta plaques in TgCRND8 mice studied with synchrotron FTIR microspectroscopy. *Biopolymers* **2007**, *87*, 207–217.

Roach, P.; Farrar, D.; Perry, C. C. Interpretation of protein adsorption: surface-induced conformational changes. *J. Am. Chem. Soc*. **2005**, *127*, 8168–8173.

Rosen, D. R.; Siddique, T.; Patterson, D.; Figlewicz, D. A.; Sapp, P.; Hentati, A.; Donaldson, D.; Goto, J.; O'Regan, J. P.; Deng, H. X. Mutations in Cu/Zn superoxide dismutase gene are associated with familial amyotrophic lateral sclerosis. *Nature* **1993**, *362*, 59–62.

Rosenblum, W. I.; Ghatak, N. R. Lewy bodies in the presence of Alzheimer's disease. *Arch. Neurol*. **1979**, *36*, 170–171.

Sarroukh, R.; Goormaghtigh, E.; Ruysschaert, J. M.; Raussens, V. ATR-FTIR: a "rejuvenated" tool to investigate amyloid proteins. *Biochim. Biophys. Acta* **2013**, *1828*, 2328–2338.

Saudou, F.; Finkbeiner, S.; Devys, D.; Greenberg, M. Huntingtin acts in the nucleus to induce apoptosis but death does not correlate with the formation of intranuclear inclusions. *Cell* **1998**, *95*, 55–66.

Shaw, B. F.; Lelie, H. L.; Durazo, A.; Nersissian, A. M.; Xu, G.; Chan, P. K.; Gralla, E. B.; Tiwari, A.; Hayward, L. J.; Borchelt, D. R.; Valentine, J. S.; Whitelegge, J. P. Detergent-insoluble aggregates associated with amyotrophic lateral sclerosis in transgenic mice contain primarily full-length, unmodified superoxide dismutase-1. *J. Biol. Chem*. **2008**, *283*, 8340–8350.

Shivu, B.; Seshadri, S.; Li, J.; Oberg, K. A.; Uversky, V. N.; Fink, A. L. Distinct β-sheet structure in protein aggregates determined by ATR-FTIR spectroscopy. *Biochemistry* **2013**, *52*, 5176–5183.

Somerville, R. A. TSE agent strains and PrP: reconciling structure and function. *Trends Biochem. Sci*. **2002**, *27*, 606–612.

Souillac, P. O.; Middaugh, C. R.; Rytting, J. H. Investigation of protein/carbohydrate interactions in the dried state. 2. Diffuse reflectance FTIR studies. *Int. J. Pharm*. **2002**, *235*, 207–218.

Spillantini, M. G.; Schmidt, M. L.; Lee, V. M.; Trojanowski, J. Q.; Jakes, R.; Goedert, M. Alpha-synuclein in Lewy bodies. *Nature* **1997**, *388*, 839–840.

Spillantini, M. G.; Crowther, R. A.; Jakes, R.; Cairns, N. J.; Lantos, P. L.; Goedert, M. Filamentous alpha-synuclein inclusions link multiple system atrophy with Parkinson's disease and dementia with Lewy bodies. *Neurosci. Lett*. **1998**, *251*, 205–208.

Stefani, M. Structural features and cytotoxicity of amyloid oligomers: implications in Alzheimer's disease and other diseases with amyloid deposits. *Prog. Neurobiol*. **2012**, *99*, 226–245.

Susi, H.; Byler, D. M. Fourier transform infrared study of proteins with parallel beta-chains. *Arch. Biochem. Biophys*. **1987**, *258*, 465–469.

Szczerbowska-Boruchowska, M.; Dumas, P.; Kastyak, M. Z.; Chwiej, J.; Lankosz, M.; Adamek, D.; Krygowska-Wajs, A. Biomolecular investigation of human substantia nigra in Parkinson's disease by synchrotron radiation Fourier transform infrared microspectroscopy. *Arch. Biochem. Biophys*. **2007**, *459*, 241–248.

The Huntington's Disease Collaborative Research Group. A novel gene containing a trinucleotide repeat that is expanded and unstable on Huntington's disease chromosomes. *Cell* **1993**, *72*, 971–983.

Thomzig, A.; Spassov, S.; Friedrich, M.; Naumann, D.; Beekes, M. Discriminating scrapie and bovine spongiform encephalopathy isolates by infrared spectroscopy of pathological prion protein. *J. Biol. Chem*. **2004**, *279*, 33847–33854.

Tonoki, A.; Kuranaga, E.; Ito, N.; Nekooki-Machida, Y.; Tanaka, M.; Miura, M. Aging causes distinct characteristics of polyglutamine amyloids *in vivo*. *Genes. Cells*. **2011**, *16*, 557–564.

Vallée, A.; Humblot, V.; Méthivier, C.; Dumas, P.; Pradier, C. M. Modifying protein adsorption by layers of glutathione pre-adsorbed on Au(111). *J. Phys. Condens. Matter*. **2011**, *23*, 484002.

Vonsattel, J. P.; Myers, R. H.; Stevens, T. J.; Ferrante, R. J.; Bird, E. D.; Richardson, E. P. Neuropathological classification of Huntington's disease. *J. Neuropathol. Exp. Neurol*. **1985**, *44*, 559–577.

Wang, Q.; Kretlow, A.; Beekes, M.; Naumann, D.; Miller, L. In situ characterization of prion protein structure and metal accumulation in scrapie-infected cells by synchrotron infrared and X-ray imaging. *Vib. Spectrosc*. **2005**, *38*, 61–69.

Yamaguchi, H.; Hirai, S.; Morimatsu, M.; Shoji, M.; Harigaya, Y. Diffuse type of senile plaques in the brains of Alzheimer-type dementia. *Acta Neuropathol*. **1988**, *77*, 113–119.

Zandomeneghi, G.; Krebs, M.; McCammon, M.; Fändrich, M. FTIR reveals structural differences between native beta-sheet proteins and amyloid fibrils. *Protein Sci*. **2004**, *13*, 3314–3321.

## Bionotes



**Guylaine Hoffner**
Laboratoire de Physiologie Cérébrale, Centre National de la Recherche Scientifique, Université Paris Descartes, 45 rue des Saints Pères, 75006 Paris, France,
**guylaine.hoffner@parisdescartes.fr**

Guylaine Hoffner obtained her PhD at the Denis Diderot University (Paris, France) on the study of the interaction of huntingtin with microtubules and its aggregation in Huntington disease. She

worked as a postdoctoral fellow at Ecole Polytechnique (Palaiseau, France), where she developed a mass spectrometric method for the quantification of a potential biomarker in neurological diseases. She is now an INSERM research scientist working at the Paris Descartes University (France), where she studies protein aggregation in Huntington disease by biochemical and biophysical techniques.



**William André**
Synchrotron SOLEIL, 91192 Saint-Aubin, France

William André obtained his PhD from Université Paris Descartes in 2012. He studied the structural polymorphism of the protein aggregates associated with Huntington's disease. He also characterized the substrates of cerebral transglutaminase, which are Ca2+-dependent enzymes possibly involved in Huntington's disease. He now holds a postdoctoral position at SOLEIL synchrotron on the infrared beam line, where he studies the effect of the cellular environment on the development of pulmonary arterial hypertension.



**Christophe Sandt**
Synchrotron SOLEIL, 91192 Saint-Aubin, France

Christophe Sandt holds a PhD in biophysics from the Reims University, France, on the identification of pathogenic microorganisms by FTIR microspectroscopy. He worked as a postdoc in the Chemistry Department of Montréal and of Saint Francis Xavier Universities, Canada, on the penetration of biocides in bacterial biofilms by FTIR-ATR spectroscopy and FTIR imaging and on bacterial biofilms composition using Raman microspectroscopy. He is now a scientist at the infrared beamline SMIS at synchrotron SOLEIL, and his main line of work is developing FTIR microspectroscopy for cellular biology applications.



**Philippe Djian**
Laboratoire de Physiologie Cérébrale, Centre National de la Recherche Scientifique, Université Paris Descartes, 45 rue des Saints Pères, 75006 Paris, France,
**philippe.djian@parisdescartes.fr**

Philippe Djian obtained an MD degree from the Université de Nice, France. He was a postdoctoral fellow in the department of Cell Biology at Harvard Medical School. He then became Directeur de Recherche at the CNRS in Paris. He was director of the Neuroscience Institute and of the laboratory of genetic regulation and genetic diseases at the Université Paris Descartes from 2000 to 2013. His research interests include diseases of polyglutamine expansion and the study of zinc finger proteins in development.